Supplementary Information (SI) for Nanoscale.

Supplementary material

Defect-Assisted Vertical Proton Channels in Highly Oriented Bismuth Strontium Tantalum Oxide Nanosheet Laminar Films

Xiang Sun, Mohammad Atiqur Rahman, Satsuki Tomatsu, Yuichi Sakuda, Kazuto Hatakeyama, and Shintaro Ida*

Institute of Industrial Nanomaterials (IINa), Kumamoto University, Kumamoto 860-8555, Japan Email: ida-s@ kumamoto-u.ac.jp

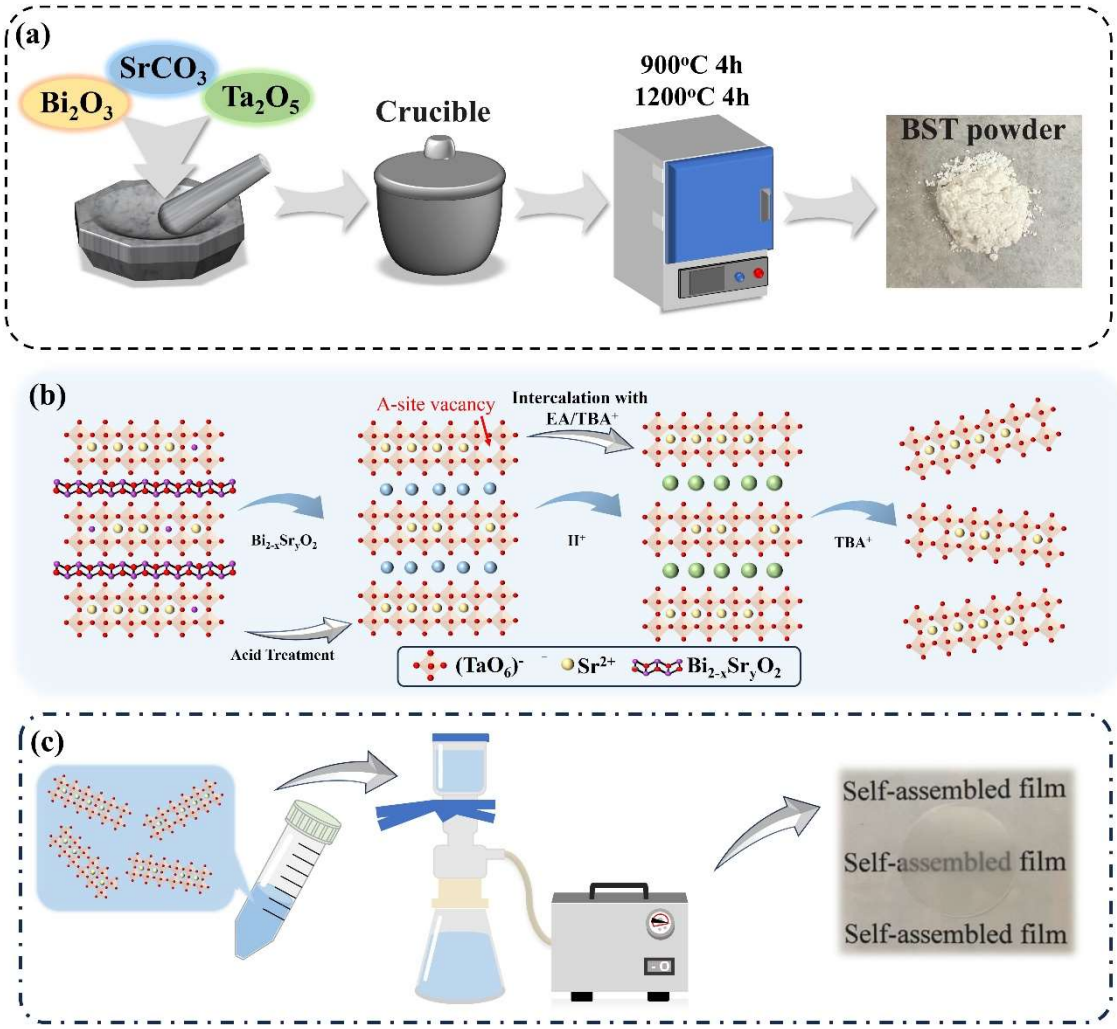

Figure S1. (a) Schematic illustration of the preparation of BST powder via solid-state method. (b) Schematic illustration of the acid-treatment induced A-site vacancy and subsequent EA/TBA^+ intercalation process. (c) Schematic illustration of the vacuum-assisted process.

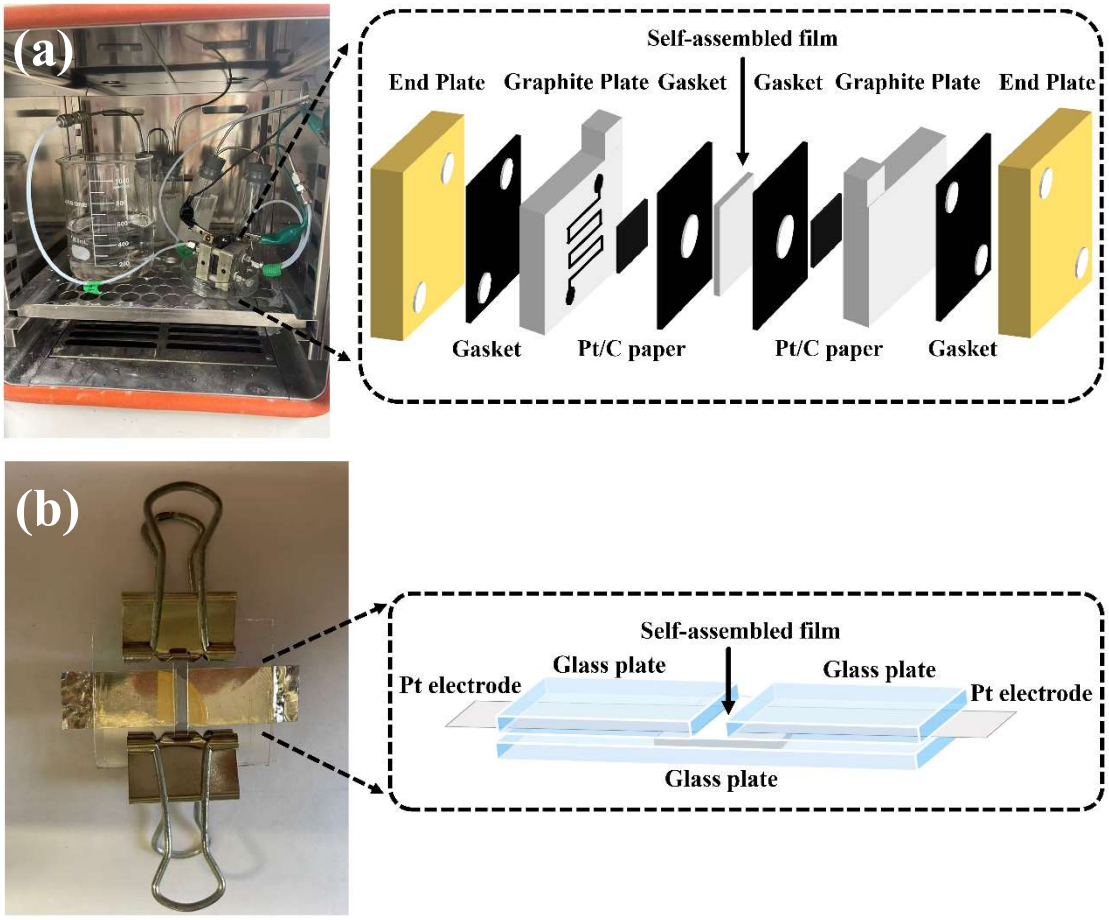

Figure S2. Photographs and schematic illustrations of proton conduction test setup. (a) out-of-plane direction, (b) In-plane direction.

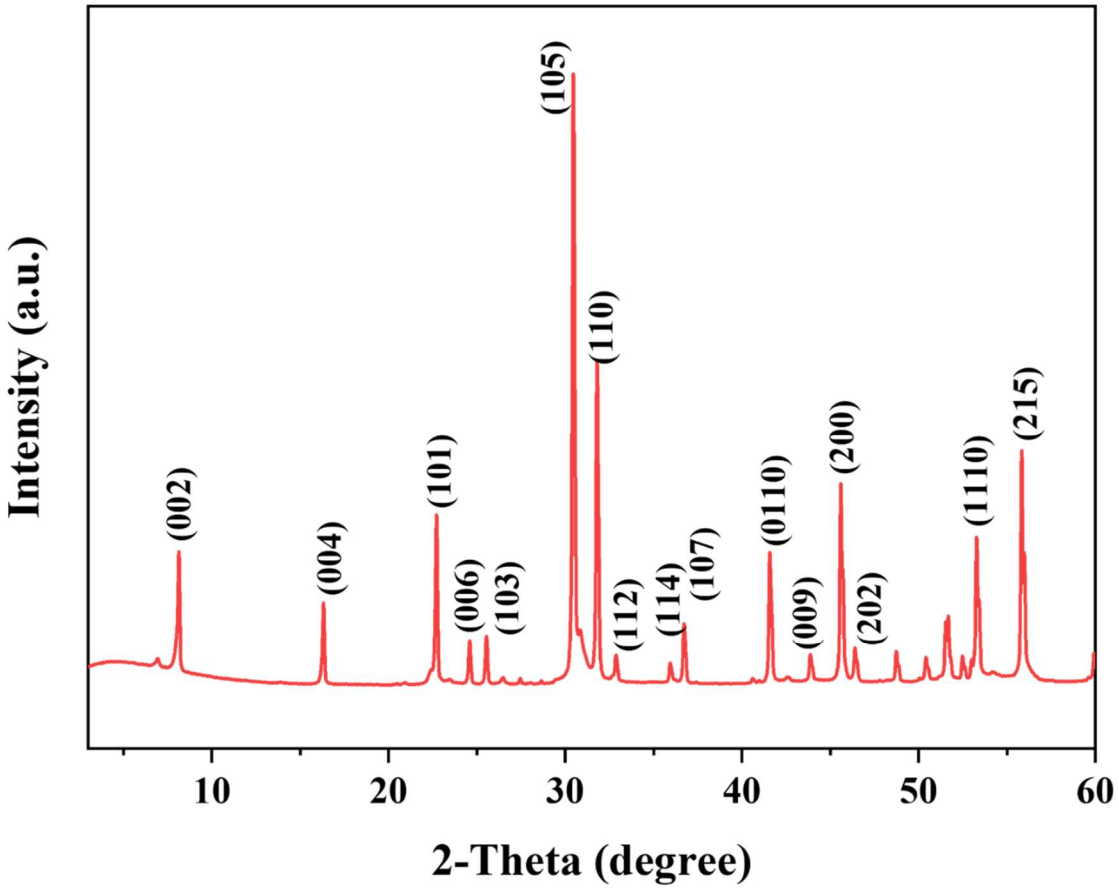

Figure S3. XRD images of original $K_2SrTa_2O_7$.

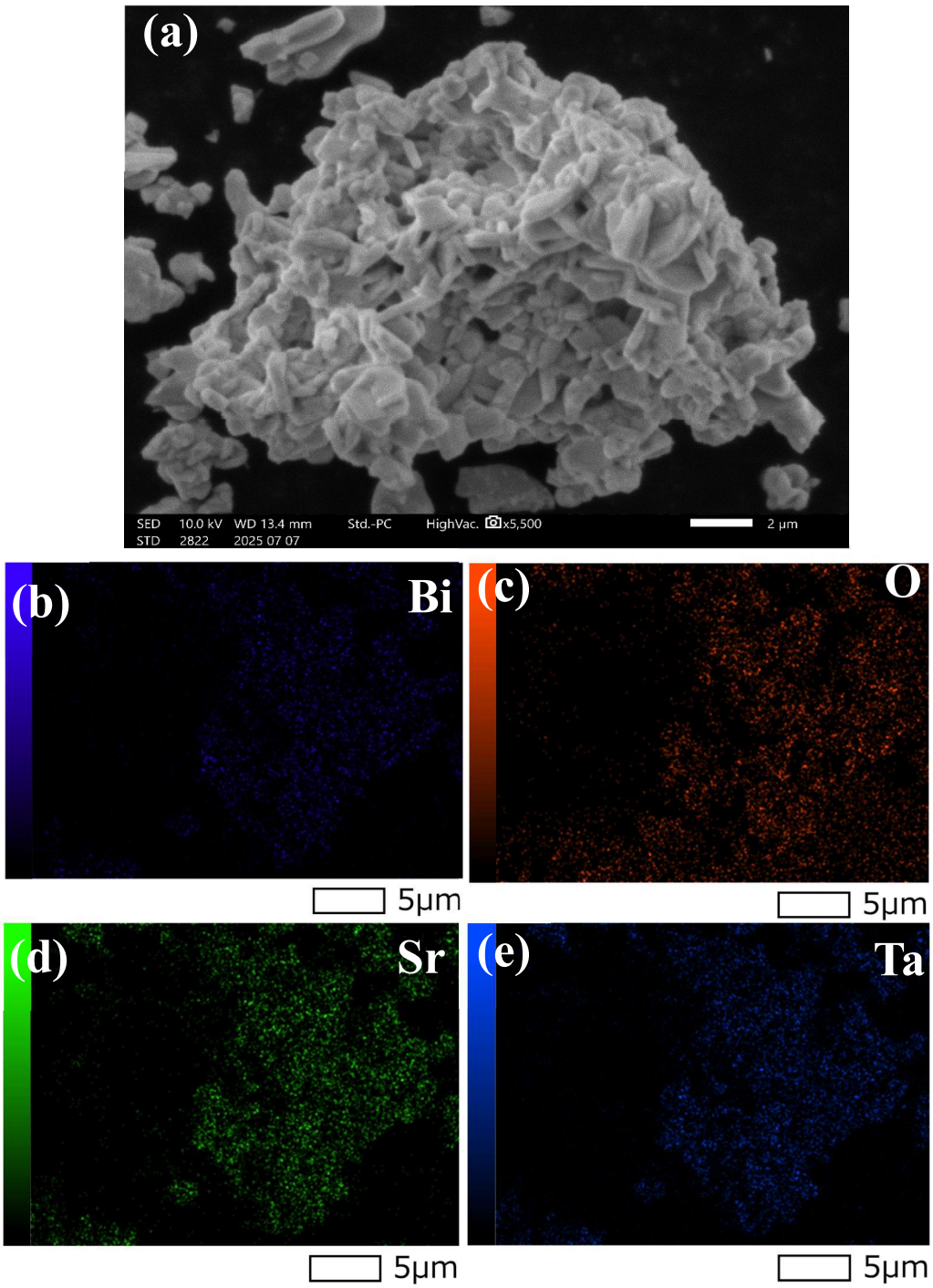

Figure S4. EDS elemental mapping of the original $Bi_2SrTa_2O_7$ (a) SEM image, (b)–(e) the corresponding elemental mapping of Bi, O, Sr and Ta, respectively.

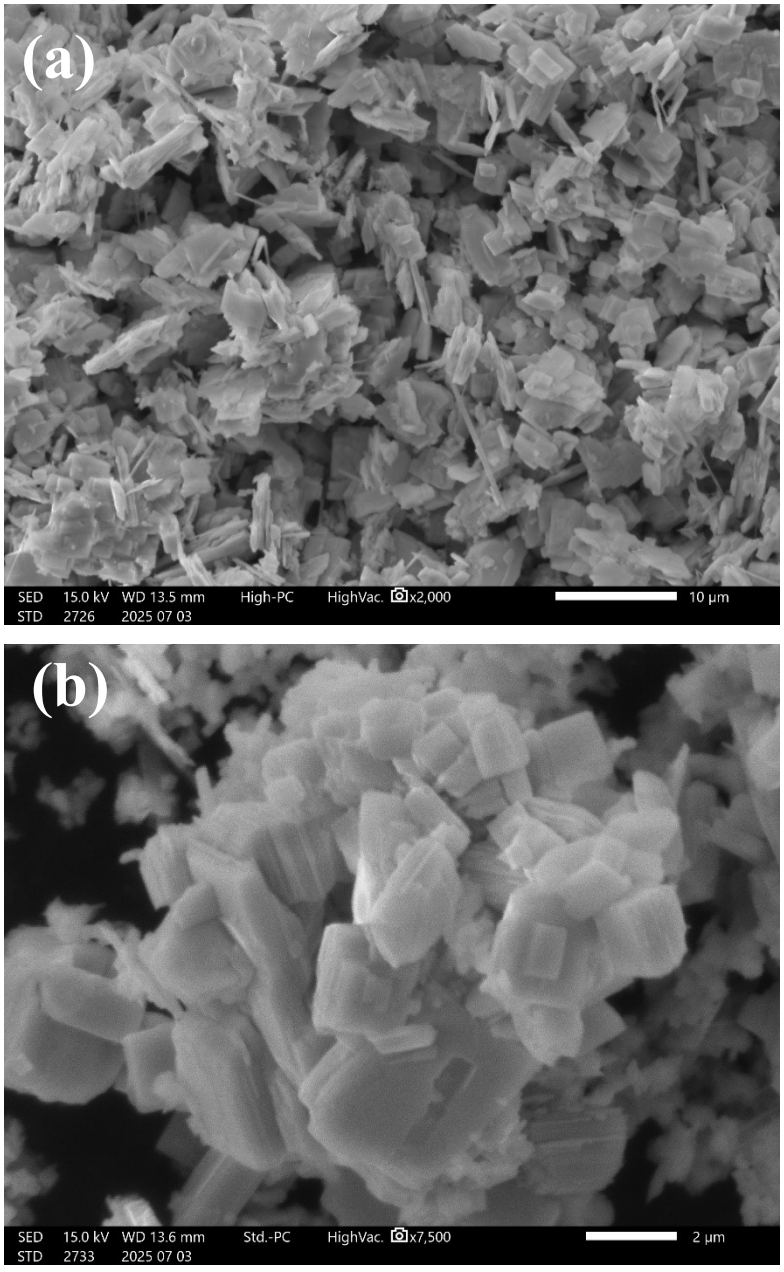

Figure S5. SEM images of original $K_2SrTa_2O_7$ (a) low magnification and (b) high magnification.

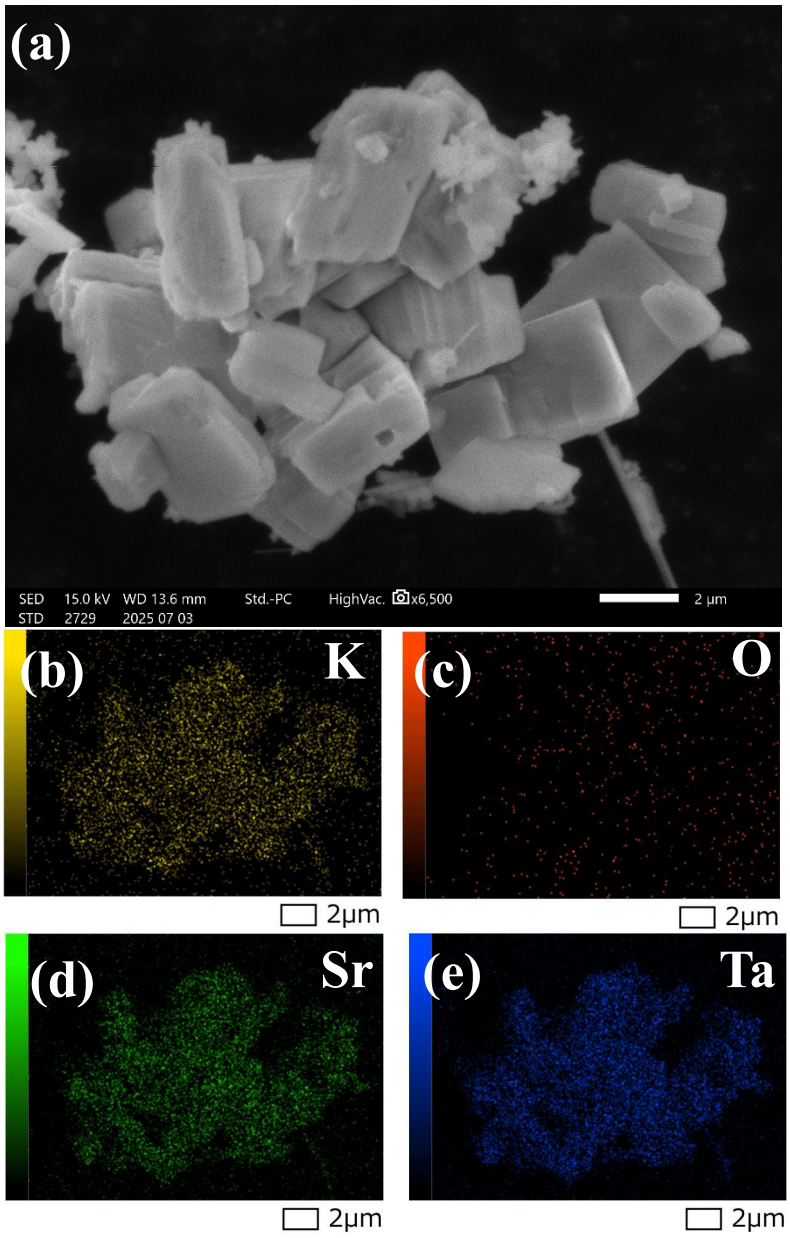

Figure S6. EDS elemental mapping of the original $K_2SrTa_2O_7$ (a) SEM image, (b)–(e) the corresponding elemental mapping of K, O, Sr and Ta, respectively.

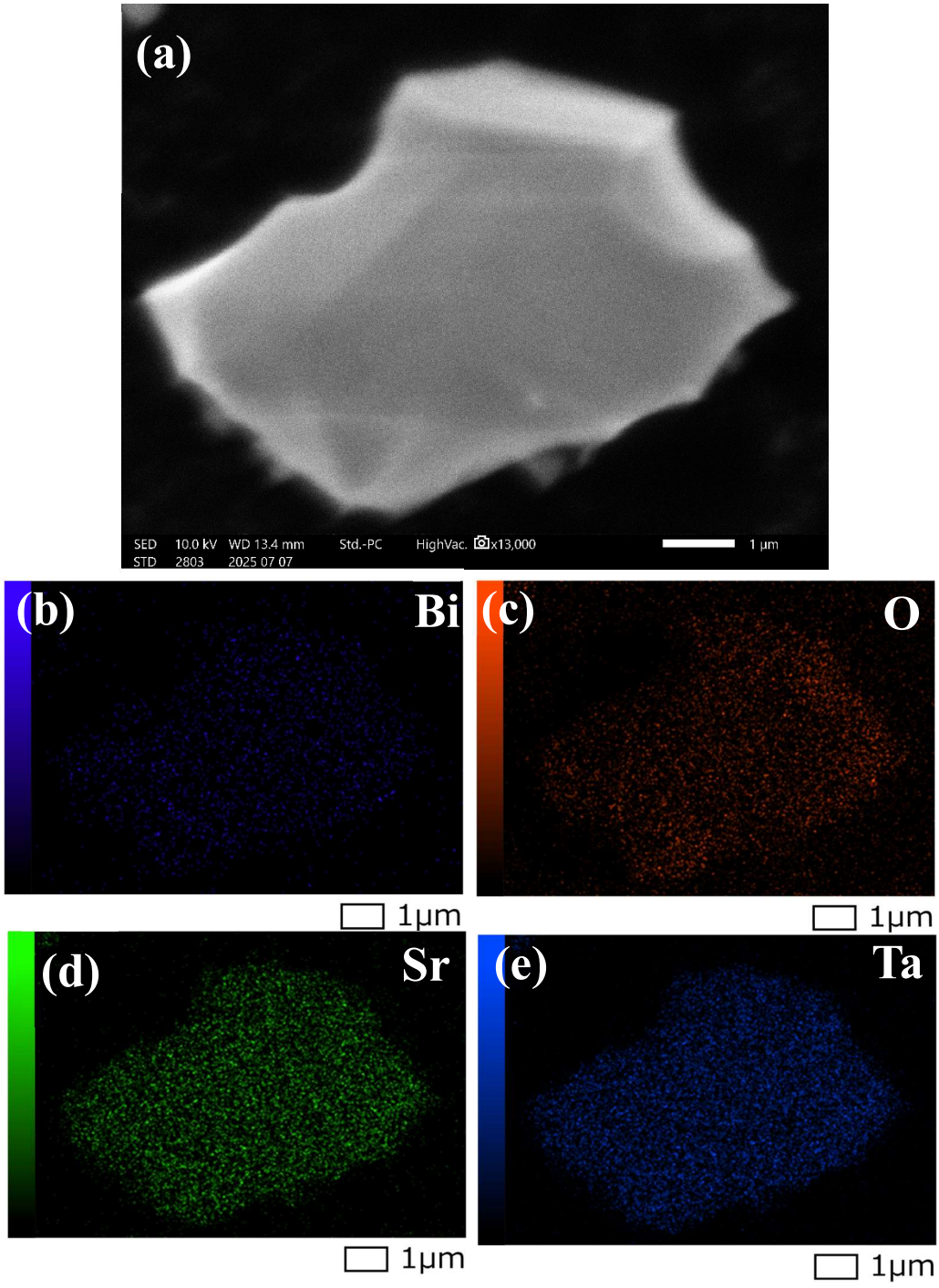

Figure S7. EDS elemental mapping of the H-BST (a) SEM image, (b)–(e) the corresponding elemental mapping of Bi, O, Sr and Ta, respectively.

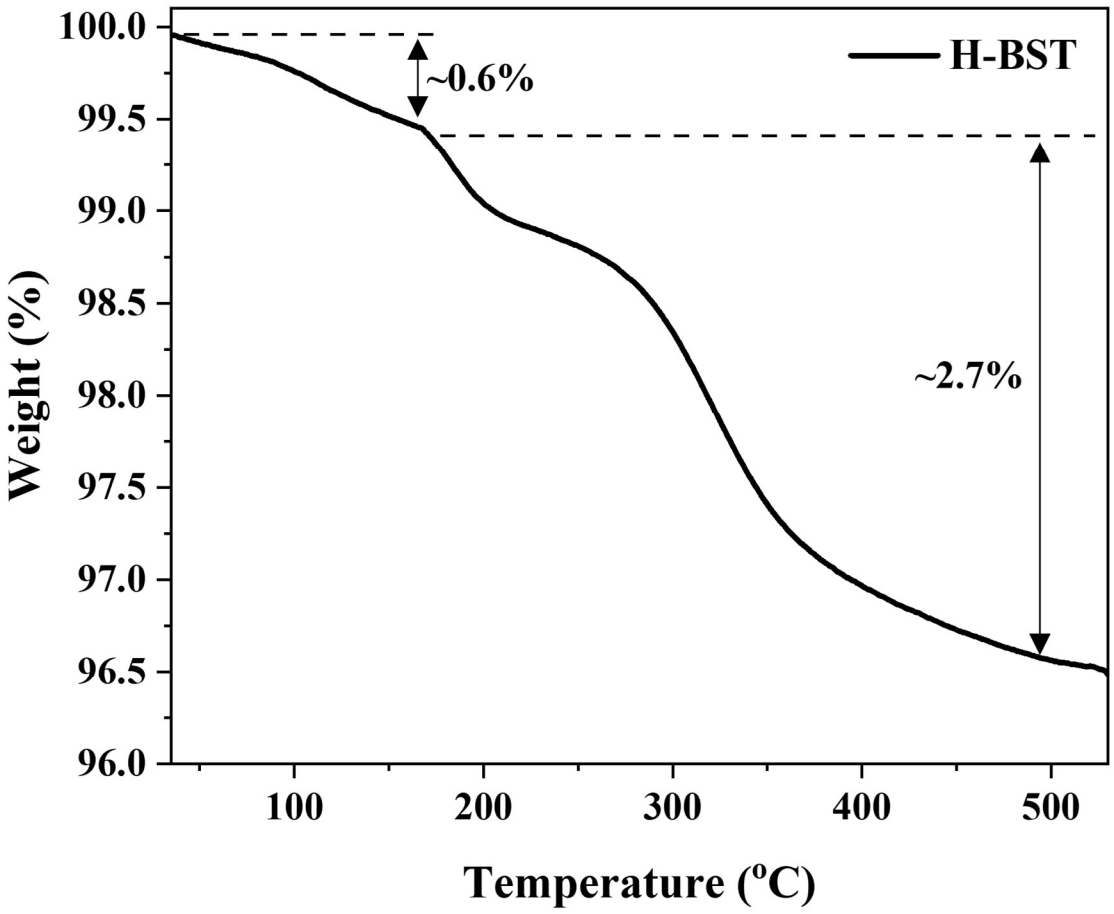

Figure S8. TGA curve of H-BST heated air atmosphere.

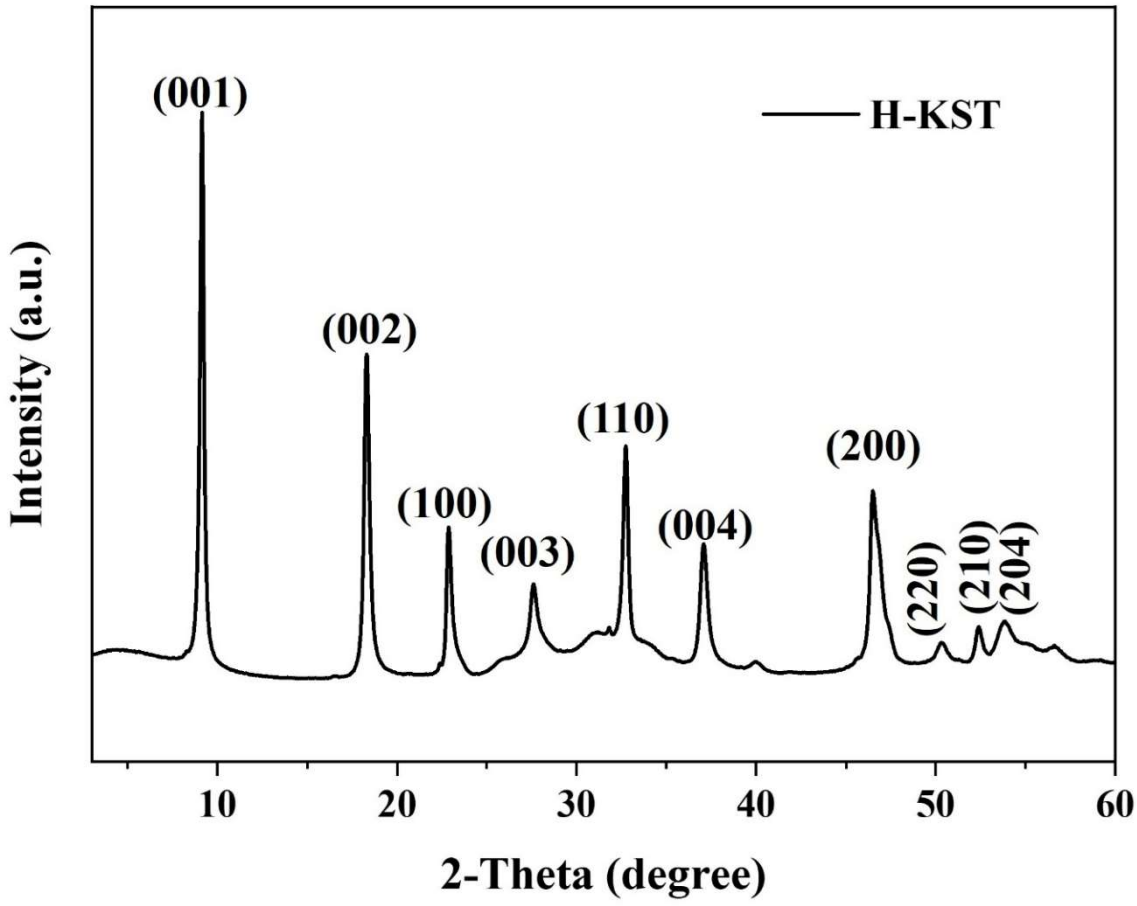

Figure S9. XRD images of H-KST.

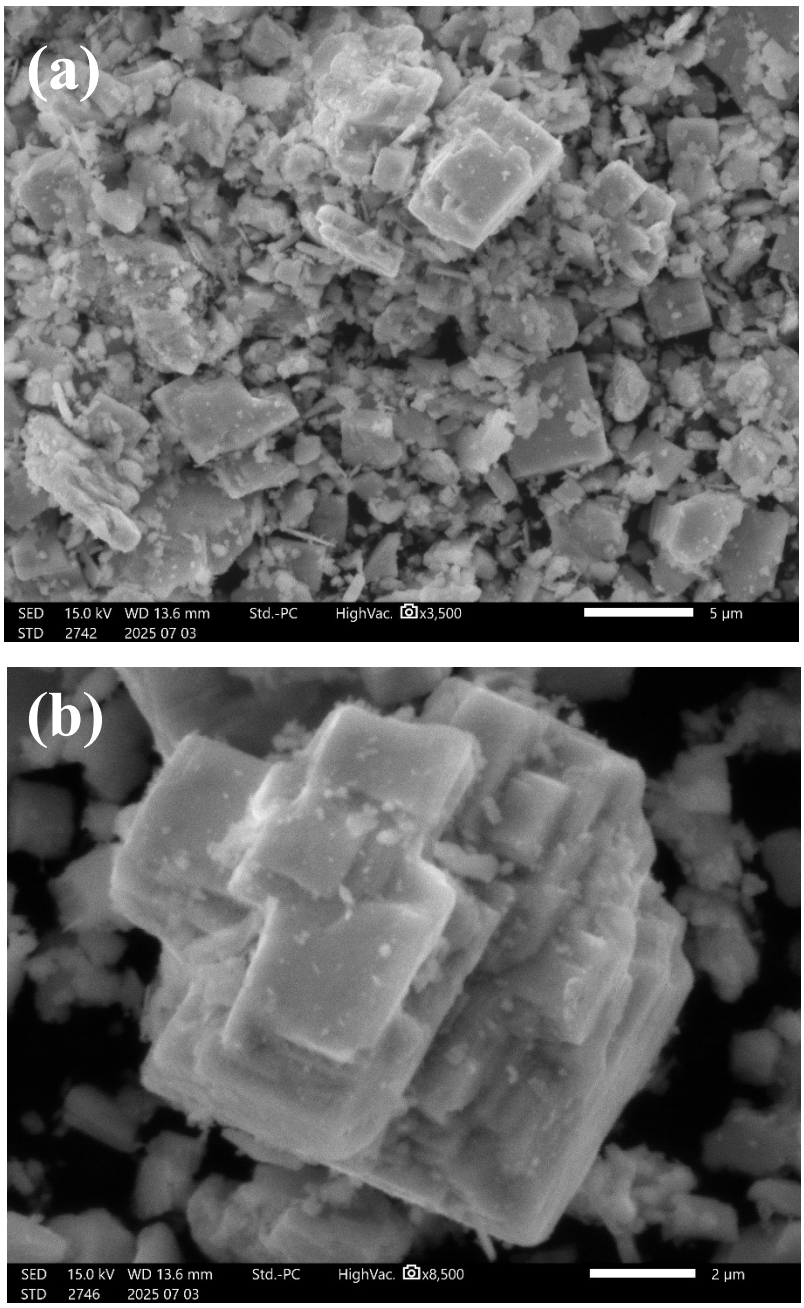

Figure S10. SEM images of H-KST (a) low magnification and (b) high magnification.

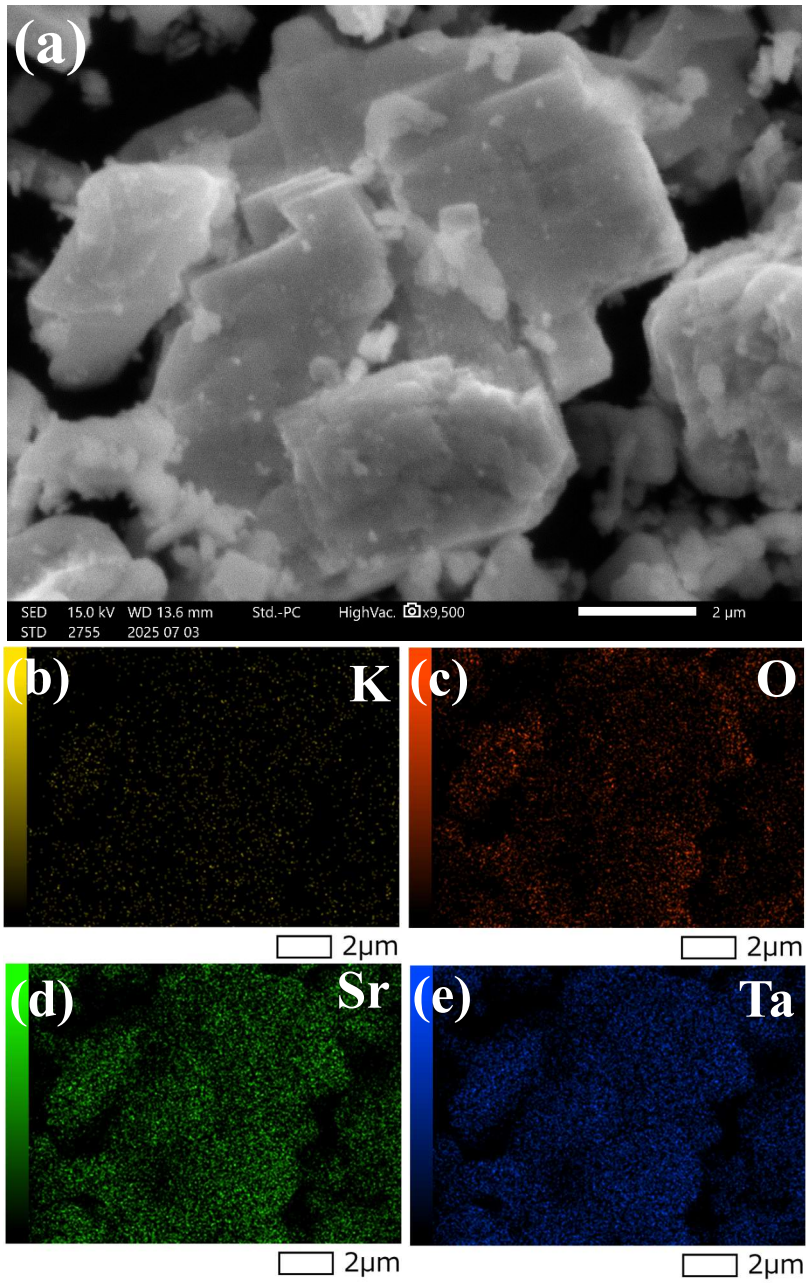

Figure S11. EDS elemental mapping of the H-KST (a) SEM image, (b)–(e) the corresponding elemental mapping of K, O, Sr and Ta, respectively.

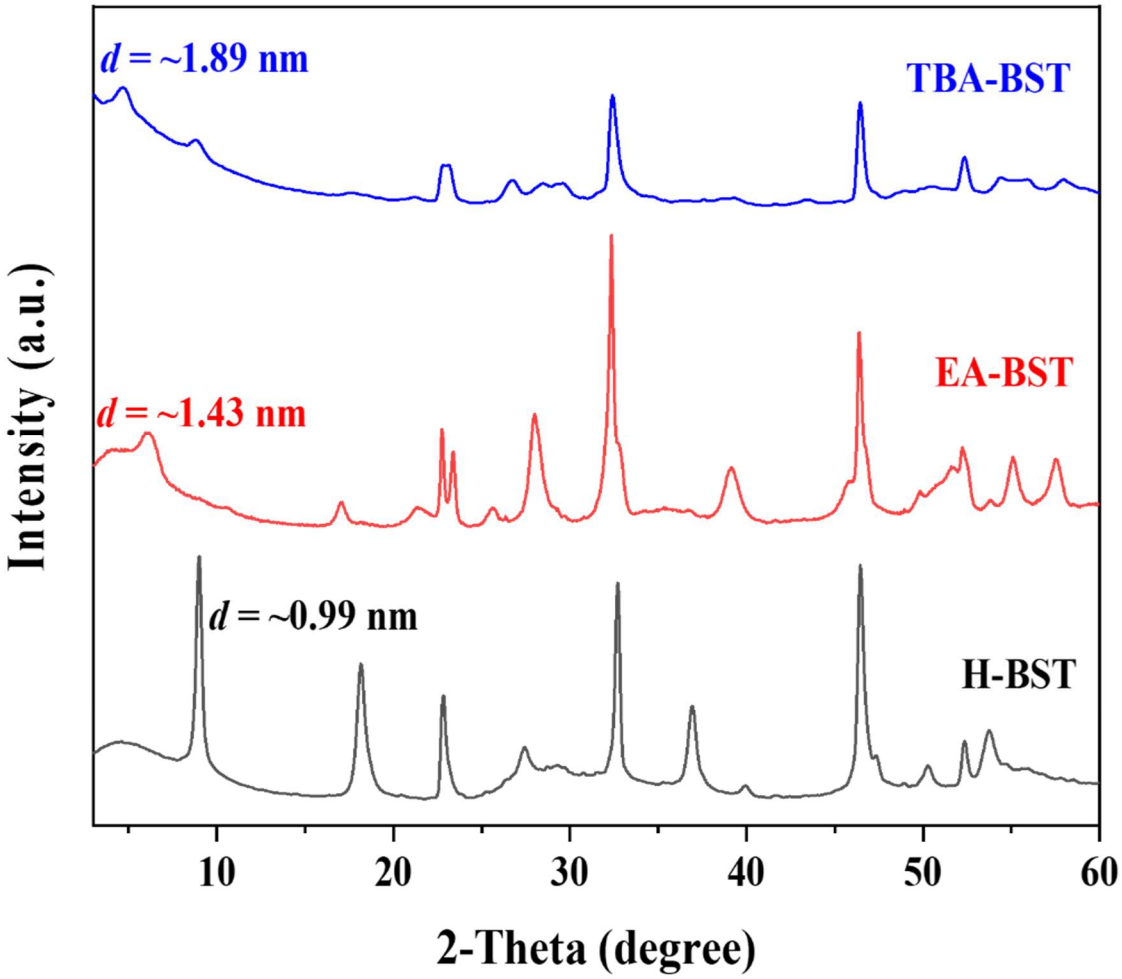

Figure S12. Summary of XRD patterns of H-BST (black line), EA-BST (red line) and TBA-BST (blue line).

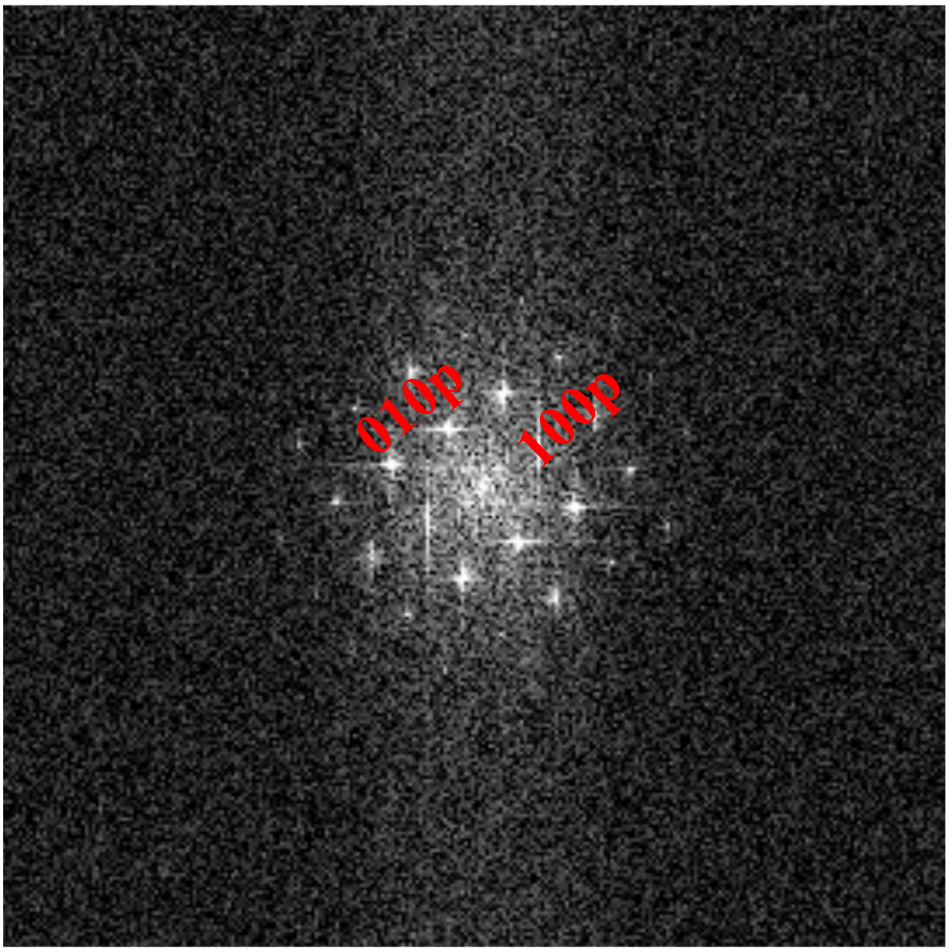

Figure S13. Corresponding FFT pattern of the $[Sr_{0.70}Bi_{0.21}\square_{0.10}Ta_2O_7]^{2-}$ nanosheet.

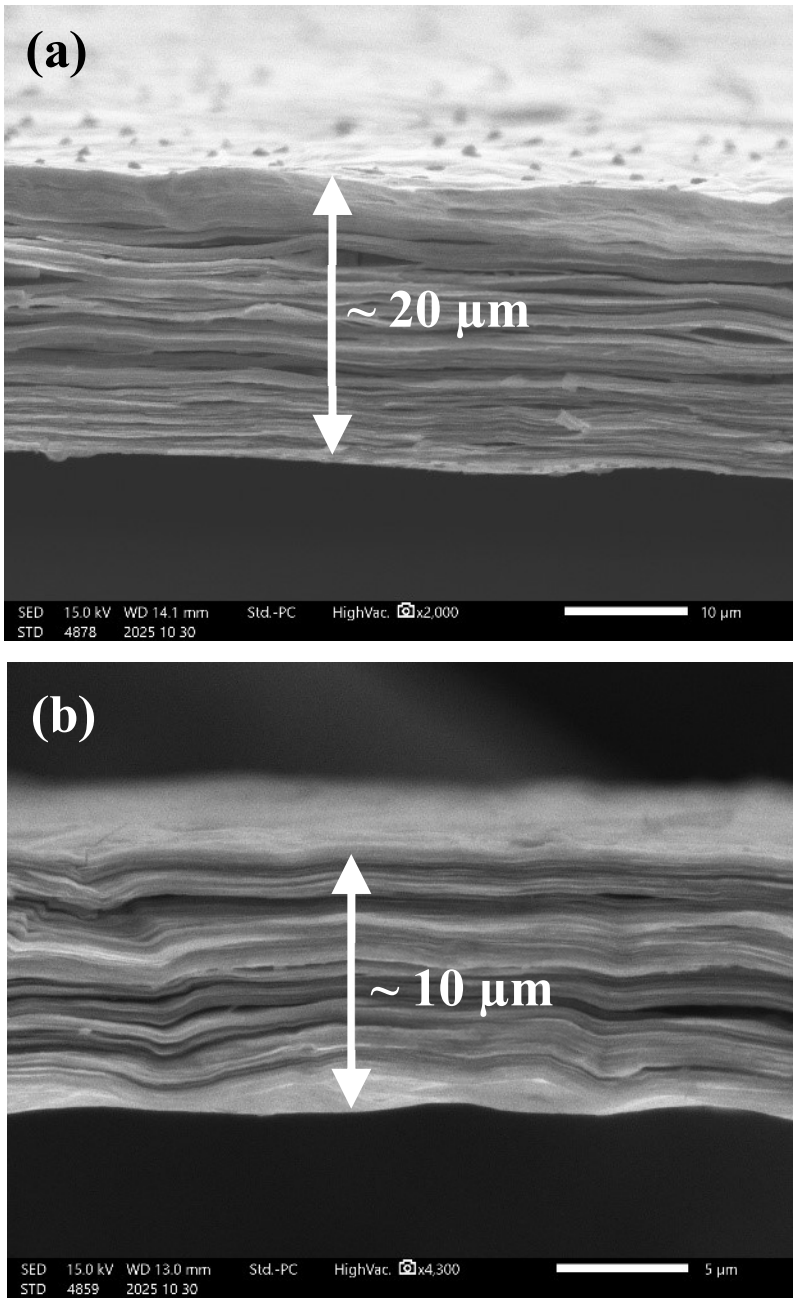

Figure S14. Cross-sectional SEM image of the $[Sr_{0.70}Bi_{0.21}\square_{0.10}Ta_2O_7]^{2-}$ self-assembled membrane with different thickness, (a) ~20 µm and (b) ~10 µm.

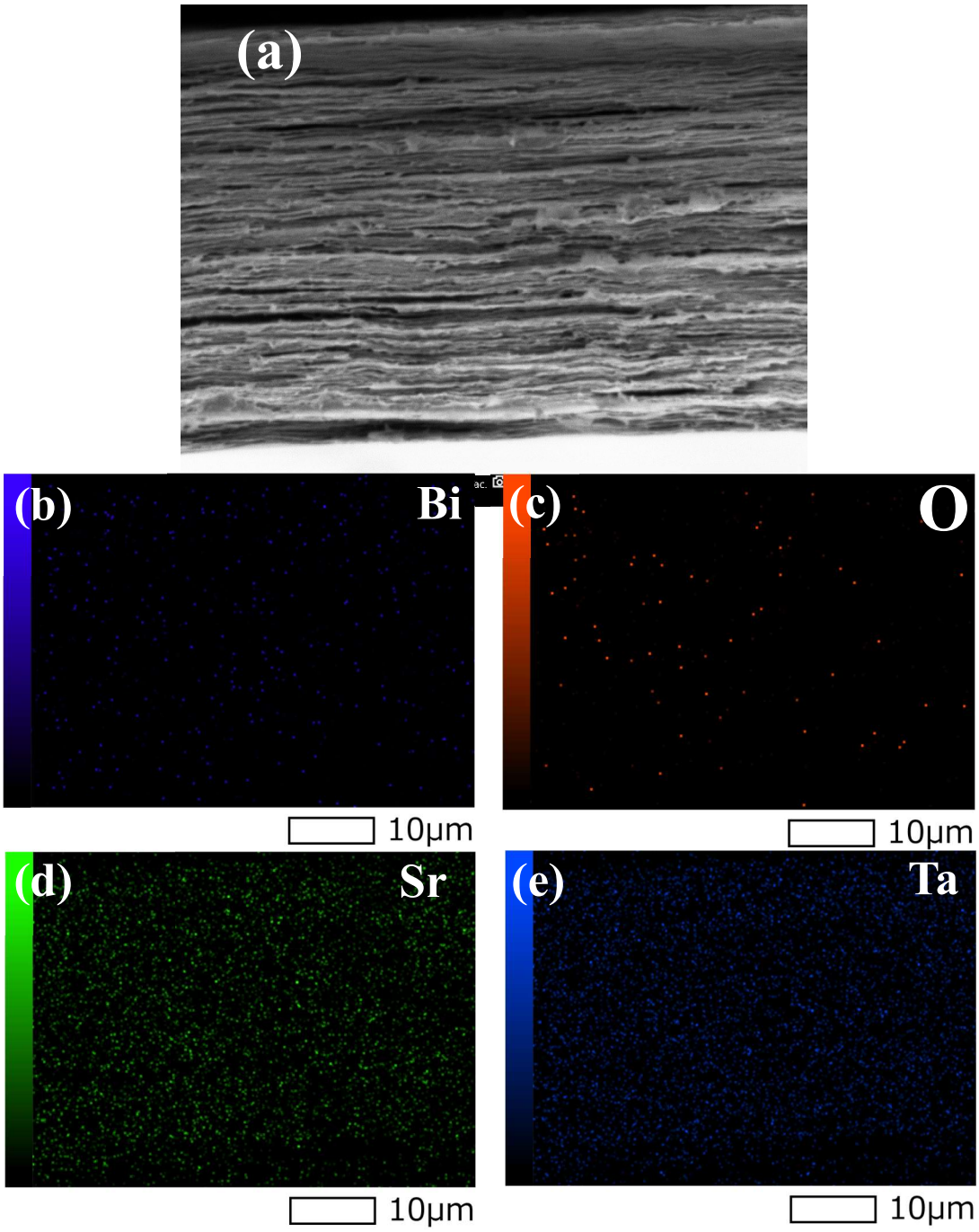

Figure S15. EDS elemental mapping of the $[Sr_{0.70}Bi_{0.21}\square_{0.10}Ta_2O_7]^{2-}$ self-assembled membrane (a) SEM image, (b)–(e) the corresponding elemental mapping of Bi, O, Sr and Ta, respectively.

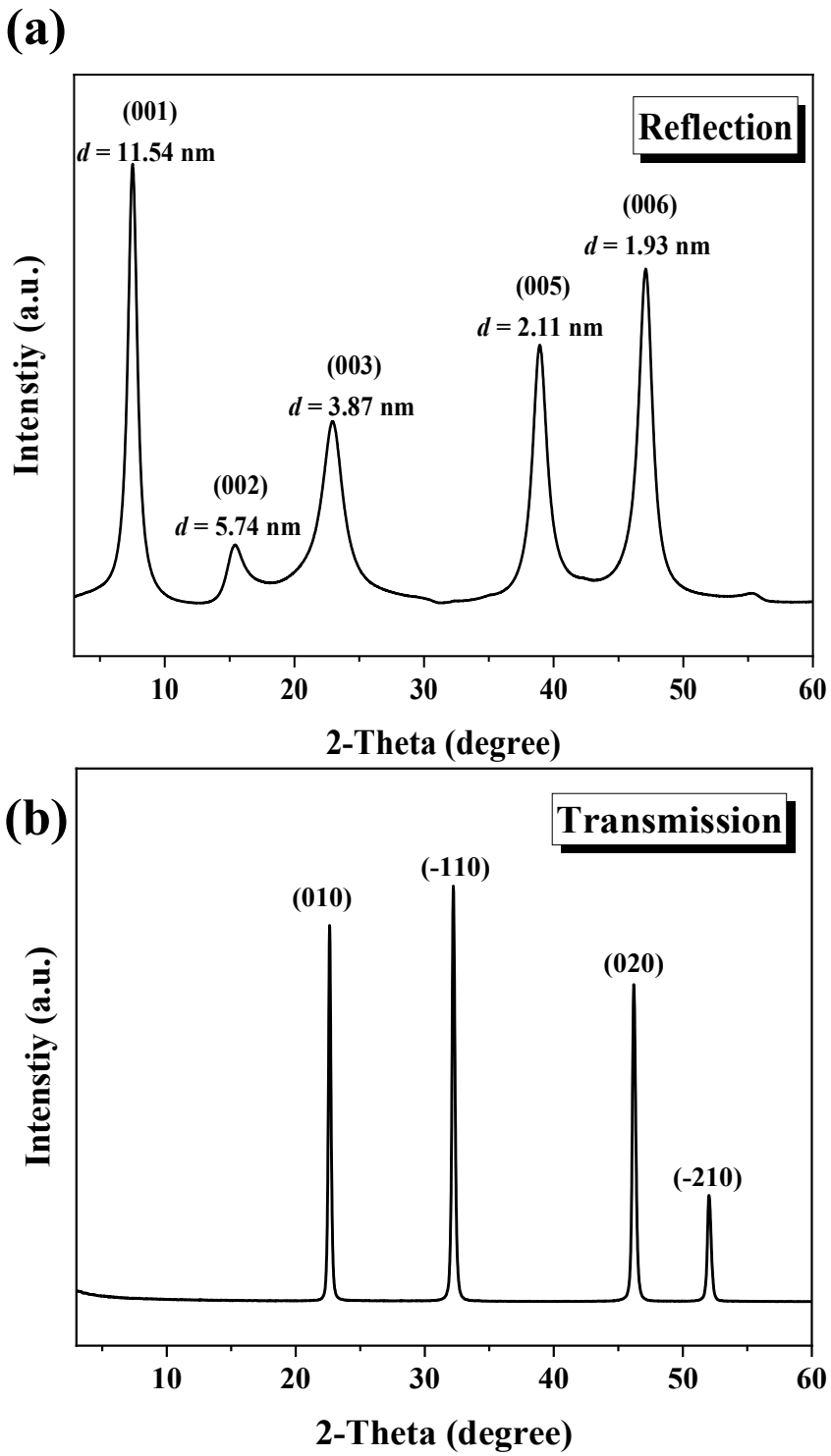

Figure S16. (a) Reflection and (b) transmission XRD images of $[SrTa_2O_7]^{2-}$ self-assembled membrane.

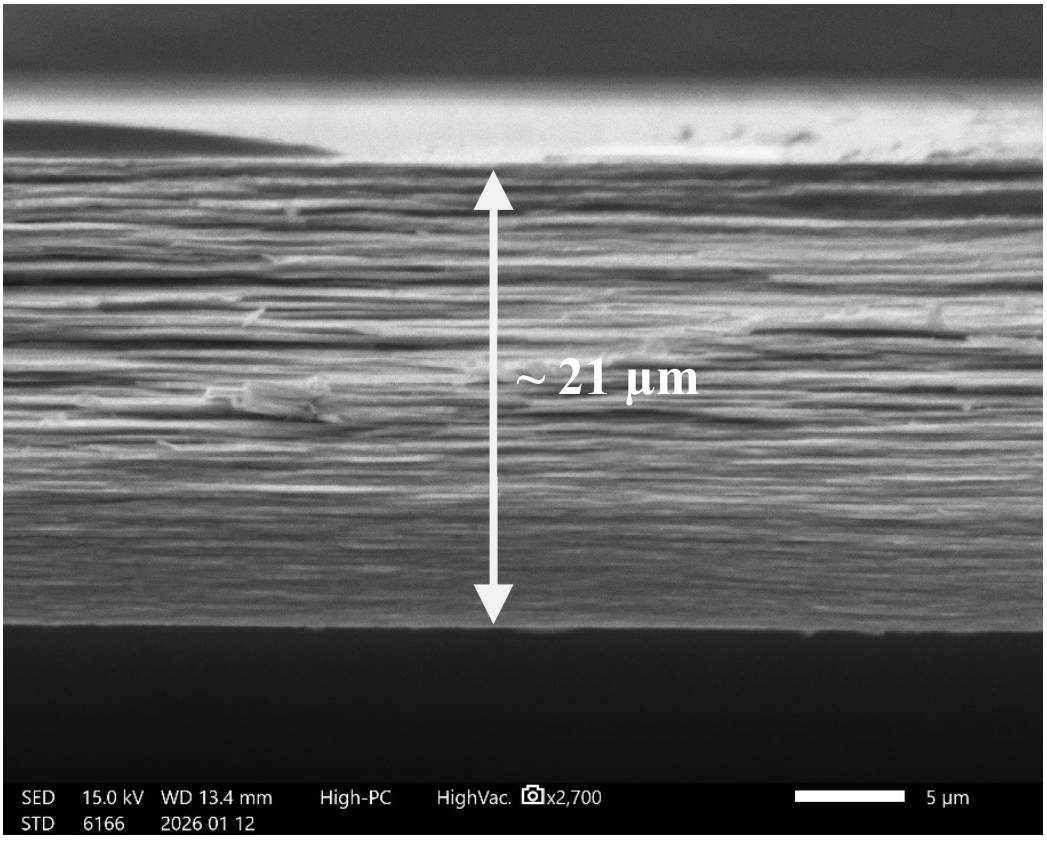

Figure S17. Cross-sectional SEM image of $[SrTa_2O_7]^{2-}$ self-assembled membrane.

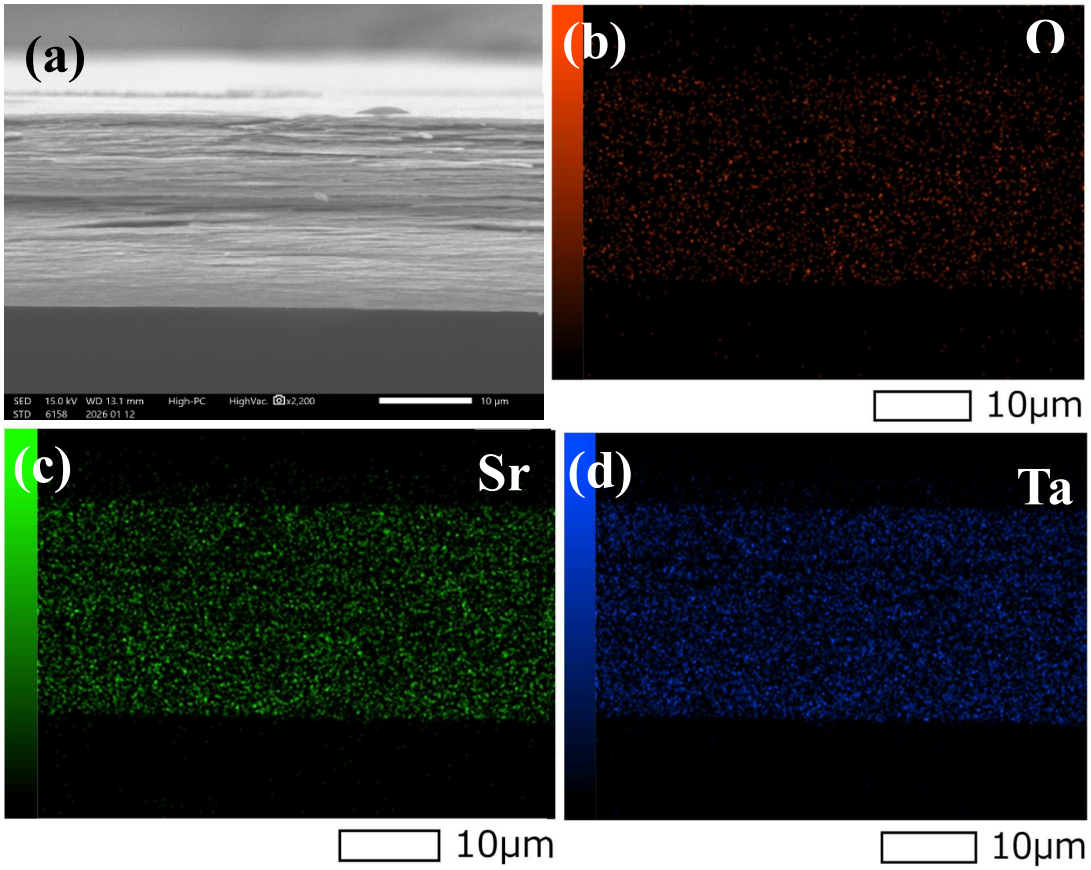

Figure S18. EDS elemental mapping of the $[SrTa_2O_7]^{2-}$ self-assembled membrane: (a) SEM image, (b)–(d) the corresponding elemental mapping of O, Sr and Ta, respectively.

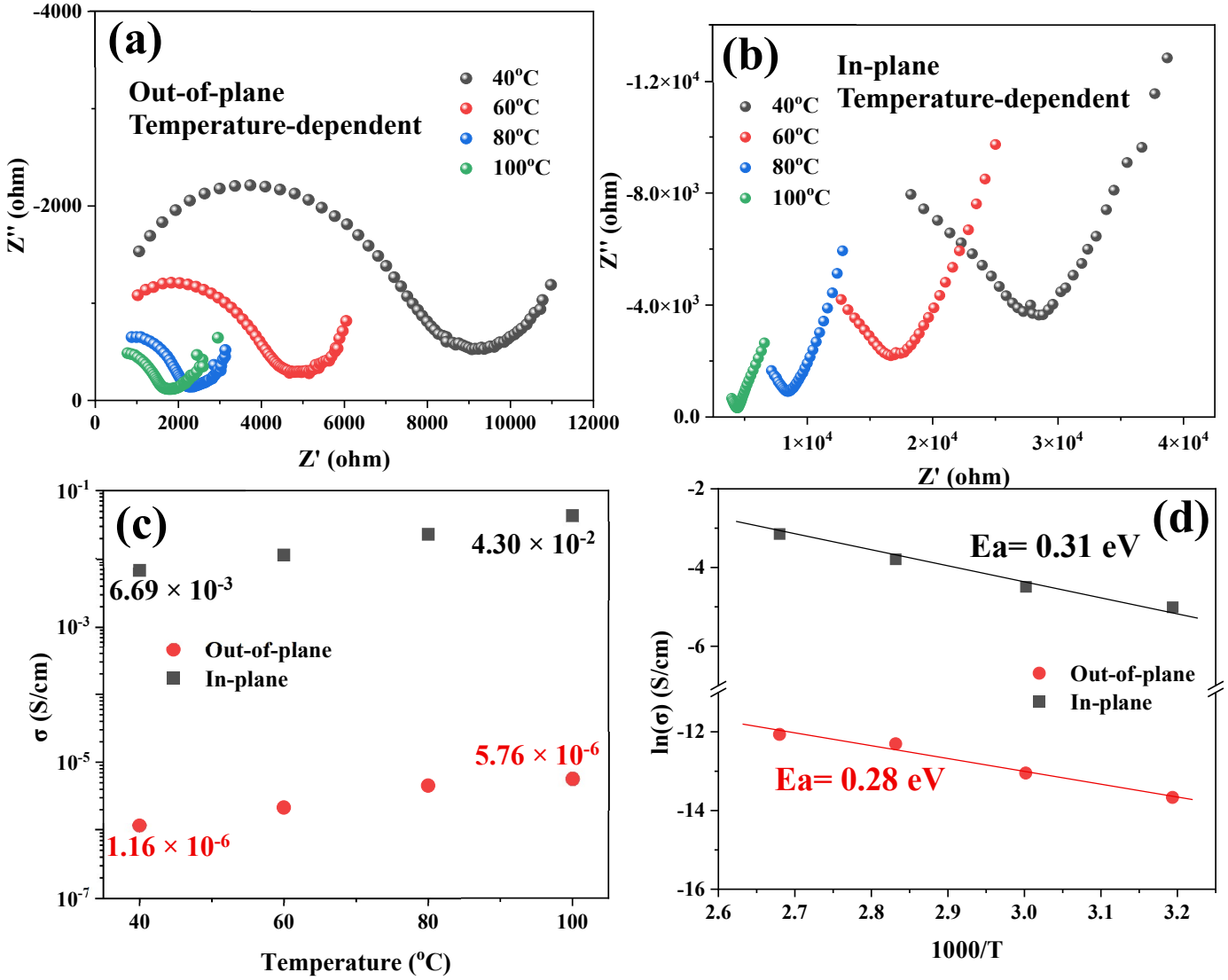

Figure S19. Temperature-dependent proton conducting property of $[SrTa_2O_7]^{2-}$ self-assembled membranes at 100% RH. (a) Nyquist plot of out-of-plane direction at 40, 60, 80 100 °C. (b) Nyquist plot of in-plane direction at 40, 60, 80 100 °C. (c) Comparison of proton conductivity (σ) in the out-of-plane and in-plane directions. (d) Arrhenius plot of proton conductivity of $SrTa_2O_7$ self-assembled membranes in the out-of-plane and in-plane directions.